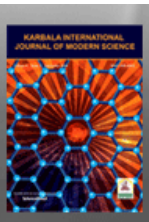
Karbala International Journal of Modern Science

Manuscript 3356

Classification and removal of hazy images based on a transmission fusion strategy using the Alexnet network

Roa'a M. Al_airaji

Haider TH. Salim ALRikabi

Rula Kamil

Classification and removal of hazy images based on a transmission fusion strategy using the Alexnet network

Abstract

Outdoor images are used in many domains, such as surveillance, geospatial mapping, and autonomous vehicles. The occurrence of noise in outdoor images is a widely observed phenomenon. They are primarily attributed to extreme natural and manufactured meteorological conditions, such as haze, smog, and fog. In autonomous vehicle navigation, recovering the ground truth image is essential, enabling the system to make more informed decisions. Accurate air-light and transmission map calculation is vital in recovering the ground truth image. An efficient approach for image dehazing that utilizes the mean channel prior (MCP) is presented in this paper to estimate the transmission map, followed by Gamma transformation to correct the transmission map obtained by MCP. This paper presents two novel contributions: first, an Alexnet network transfer model classification of hazy images as a preprocessing, and second, an efficient image dehazing based on an image fusion strategy. In the image dehazing stage, the transmission map estimated by the mean channel is altered with Gamma correction first. Then, the initial transmission map and its modified copy are combined using the weighted average fusion technique to retain the information in the initial transmission map. Additionally, the fused transmission map undergoes filtration using a guided filter to mitigate block and halo artifacts within the dehazed image. Lastly, the dehazed image is recovered using the improved transmission map by utilizing an optical scattering model. The proposed Alexnet network transfers algorithm significantly and decreases the quantity of training data required compared to the traditional classification algorithm. In addition, the network's classification accuracy can reach 98%. The proposed image dehazing showed better performance in terms of computational time, natural image quality evaluator (NIQE) index, peak-signal-to-noise ratio (PSNR), and structural similarity index (SSIM) than that of existing methods.

Keywords

Image dehazing; Hazy image classification; Alexnet network; Mean channel prior; Gamma correction; Image fusion

RESEARCH PAPER

Classification and Removal of Hazy Images Based on a Transmission Fusion Strategy Using the Alexnet Network

Roa'a M. Al_airaji [a,*], Haider T.H.S. ALRikabi [b], Rula Kamil [a]

[a] Department of Software, College of Information Technology, University of Babylon, Babylon, Iraq
[b] Department of Electrical Engineering, College of Engineering, Wasit University, Al Kut, Iraq

Abstract

Outdoor images are used in many domains, such as surveillance, geospatial mapping, and autonomous vehicles. The occurrence of noise in outdoor images is a widely observed phenomenon. They are primarily attributed to extreme natural and manufactured meteorological conditions, such as haze, smog, and fog. In autonomous vehicle navigation, recovering the ground truth image is essential, enabling the system to make more informed decisions. Accurate air-light and transmission map calculation is vital in recovering the ground truth image. An efficient approach for image dehazing that utilizes the mean channel prior (MCP) is presented in this paper to estimate the transmission map, followed by Gamma transformation to correct the transmission map obtained by MCP. This paper presents two novel contributions: first, an Alexnet network transfer model classification of hazy images as a preprocessing, and second, an efficient image dehazing based on an image fusion strategy. In the image dehazing stage, the transmission map estimated by the mean channel is altered with Gamma correction first. Then, the initial transmission map and its modified copy are combined using the weighted average fusion technique to retain the information in the initial transmission map. Additionally, the fused transmission map undergoes filtration using a guided filter to mitigate block and halo artifacts within the dehazed image. Lastly, the dehazed image is recovered using the improved transmission map by utilizing an optical scattering model. The proposed Alexnet network transfers algorithm significantly and decreases the quantity of training data required compared to the traditional classification algorithm. In addition, the network's classification accuracy can reach 98%. The proposed image dehazing showed better performance in terms of computational time, natural image quality evaluator (NIQE) index, peak-signal-to-noise ratio (PSNR), and structural similarity index (SSIM) than that of existing methods.

Keywords: Image dehazing, Hazy image classification, Alexnet network, Mean channel prior, Gamma correction, Image fusion

1. Introduction

The issue of limited visibility poses a significant challenge when trying to ascertain the exact ground truth. Recently, several researchers have made significant contributions to addressing this issue. Fog consists mostly of aerosols and fine particles suspended in the air. Fog plays a substantial role in raising the relative humidity in the atmosphere until it reaches saturation [1]. So, fog and haze, which reduce visibility, share a common origin. Numerous applications call for the automatic detection of hazy images and the application of suitable algorithms to restore the original brilliance of object detection for additional processing, such as object detection, segmentation, and different vision fields [2]. The task is difficult because the haze concentration closely relates to the object's depth [3]. Khmag et al. [4] suggested a method for dehazing a single image based on fine texture and edge preservation. This method is divided into two parts: the first part uses the mean vector L2-norm to estimate the transmission map. The second

Received 7 February 2024; revised 20 April 2024; accepted 24 April 2024.
Available online 13 June 2024

* Corresponding author.
E-mail address: sci.roaa.mohammed@uobabylon.edu.iq (R.M. Al_airaji).

https://doi.org/10.33640/2405-609X.3356

part uses the second generation of wavelet transform to enhance the transmission map. Kumar et al. [5] suggested an algorithm for calculating the transmission map-based color uniformity principle, but airlight estimation needs to be more accurate under various haze situations. The study of Gao et al. [6] is built upon the local linear integration of the subtracted layer of haze image and gamma-corrected grey image, but generalization to other images is needed. Khmag [7] suggested a method for dehazing and defogging images using transmission map estimation and second-generation wavelets. The proposed technique can handle images with multiple haze densities. It enhances the transmission map based on semi-soft thresholding and gamma transformation with the second-generation wavelet transformation.

A dehazing method based on several images taken at various polarization levels was proposed by Narasimhan and co-authors [8]. Taking multiple images simultaneously is inconvenient, even though it yields impressive results. In the past, numerous researchers have significantly improved single-image dehazing techniques. To remove haze, contrast-limited adaptive histogram equalization (CLAHE) and retinex method were used as image enhancement techniques. The results of CLAHE, which emerged for images used in medicine and has demonstrated excellent performance, could be more visually competent for hazy images [9]. Retinex theory indicates improved performance in inadequate illumination [10], whereas haze removal is entirely different and depends on the object's depth. By boosting the image's local contrast using Markov random fields, Tan proposed a novel method for removing haze from single images, but it suffers from color shift [11]. Fattal offered Independent component analysis for haze removal, but the technique takes time [12]. The transmission map was estimated based on the mean channel prior, based on the probability assumption that each space image will have at least one color channel, which is minimal or extremely close to zero. Still, the transmission map was refined using a soft mat, which took much time [2].

Many modifications were made to the traditional DCP technique to enhance the clarity of hazy images, such as using guided filters rather than soft matting for image haze removal [13]. Additionally, several changes were made, including the near-infrared images and integration of high-frequency elements [14], the use of surround filtering [15] with DCP for haze removal, and average saturation prior [16] for calculating the transmission map, respectively. Transmission map and airlight estimation were performed using linear transformation algorithms like a fast mean filter, minimum filter, and natural and geometric characteristics of outdoor images [17]; however, there needed to be more evidence of advancement over the application. Techniques like boundary constraint [18] and color attenuation prior [19] were utilized. Clear images form tight clusters of distinct colors, and all outdoor images can be characterized by a limited range of colors and form haze lines, which were utilized in literature to remove haze. The scene prior using non-local total variation (NLTV) regularization [20], adaptive wiener filter [21], saliency map [22], and reference retrieval [23] are just a few of the DCP-dependent techniques that have been developed in the past for image dehazing applications. A new method for calculating the transmission map for the sky and non-sky areas based on DCP and extension, respectively, and using sigmoid fusion was recently presented by Sahu and Seal [24]. Khmag [25] studied the problem of medium transmission inaccuracy and proposed a smoke removal strategy based on dark channel prior (DCP). According to the conventional DCP, second-generation wavelets filter (SGWs) is used to further increase ambient light in the digital image, which DCP indicates as a global constant.

Artificial intelligence techniques such as machine learning and deep learning have proven successful in various imaging applications. Cai and colleagues [26] introduced a novel deep-learning approach to de-haze from a single image called Dehaze Net. The method used a convolutional network and incorporates a bilateral rectified linear unit activation function to estimate the transmission map. Santra et al. [27] introduced a deep learning method for dehazing a single image based on a patch quality comparison. The above strategies have been helpful, but there is always room for development. In other words, most contemporary dehazing algorithms rely heavily on precisely estimating the transmission map. This paper has developed an MCP-fusion model combination to estimate the transmission map better. The developed method is based on MCP, positively affecting natural scene images. At the same time, the theory will be incorrect in areas that are too dark or bright, leading to an imprecise transmission map and over-enhancement of the recovered images. To address this issue, this paper extends the dynamic range of the low grayscale region by applying gamma correction to the MCP initial transmission map. Fortunately, Gamma correction may result in losing some information in the initial transmission map.

Furthermore, it may cause the transmission map to be imprecise in dense, hazy regions, resulting in insufficient dehazing. In light of this issue, an image

fusion technique was proposed that combines the initial transmission map with its improved version using Gamma correction. The fusion approach preserves the details of the restored image. Furthermore, the fused transmission map undergoes filtration using a guided filter to mitigate block and halo artifacts within the dehazed image. As a preprocessing unit, this article provides an Alexnet network transfer model for hazy, non-hazy image classification and image dehazing. Based on the constraints of the current methodologies in the literature, the proposed work proposes and summarizes the following main contribution:

- A hazy image classifier automatically detects hazy images. So, clear images need no preprocessing.
- A method for transmission map estimation based on image fusion is presented. This paper used the fusion method to combine the original MCP transmission map with the gamma-corrected version. It preserved the features in the transmission map and fixed the issue of further optimizing inaccurate results due to an erroneous transmission map.
- A proposed method for removing haze relies on a transmission map estimation strategy based on image fusion and an optical scattering model. The guided filter is employed in this dehazing approach to adjust the transmission map to eliminate block and halo artifacts in the final dehazed images.
- Experiments on both real-world and synthetic data sets are carried out to prove the proposed method's capability and demonstrate its efficiency over other modern techniques. The results show that the proposed strategy is superior regarding subjective visual perception and quantitative evaluation measures.

The remainder of the paper is organized as follows: Section 2 discusses the scattering model. Section 3 explains the proposed method. Section 4 discusses the comparison of results. Finally, Section 5 is included, and the conclusions are discussed.

2. Atmospheric scattering model (ASM)

File ASM can be can be mathematically expressed using Equation (1) below:

$$\mathrm{I(i,j)} = G(\mathrm{i,j}).\mathrm{t(i,j)} + \mathrm{A}(1 - \mathrm{t(i,j)}) \tag{1}$$

Where (i,j) are the pixel coordinates, I(i, j) is the irradiance of the scene (the captured hazy image), G(i, j) is the image's ground truth (the haze-free image), A is the airlight and t(i, j) is the transmission map. The transmission map depends on an object's distance from the camera lens [1].

$$t(i,j) = e^{-\beta d} \tag{2}$$

Where β is the attenuation parameter, and d (i,j) denotes the image's object depth at (i,j) coordinates. Based on the equations mentioned earlier, it can be inferred that when the object depth approaches infinity, the function t(i) converges to zero, while the function I(i) remains constant at A. When the object is positioned in the foreground, the depth of the scene is expected to be relatively shallow, resulting in Equation J(i,j) = I(i,j) for (1). If the values of two variables, namely d(i) and A, can be determined, it is possible to reconstruct the irradiance of the original scene from the deformed image. After calculating the two crucial parameters, airlight and the transmission map, the ground truth can be calculated directly as:

$$J(i) = \frac{I(i) - A}{t(i)} + A \tag{3}$$

3. Proposed method

Fig. 1 illustrates the proposed method's comprehensive structure. It can be broadly categorized into two main components: classification and restoration.

The addition of intelligence is necessary to enable automation inside any given system. To address this concern, this paper developed a classifier utilizing an Alexnet network transfer algorithm. This classifier is designed to determine whether an image has been affected by haze accurately. If the classifier's output is nearly zero, it can be inferred that the input image is high quality and can be readily utilized for subsequent processing. The classifier developed in this study demonstrates a level of precision of 97.4%. If the classifier produces a value close to one, it can be inferred that noise, such as haze or fog, has affected the collected image. This classifier facilitates the exclusion of clean images, alleviating the computational burden on the processor and obviating the need for human intervention. The technique was specifically developed to handle the input image if the classifier score exceeds a threshold of 0.6.

After the classifier, the original transmission map is generated using MCP and corrected using Gamma transform. The original transmission map and its improved form are combined via image fusion. Then, the fused transmission map is

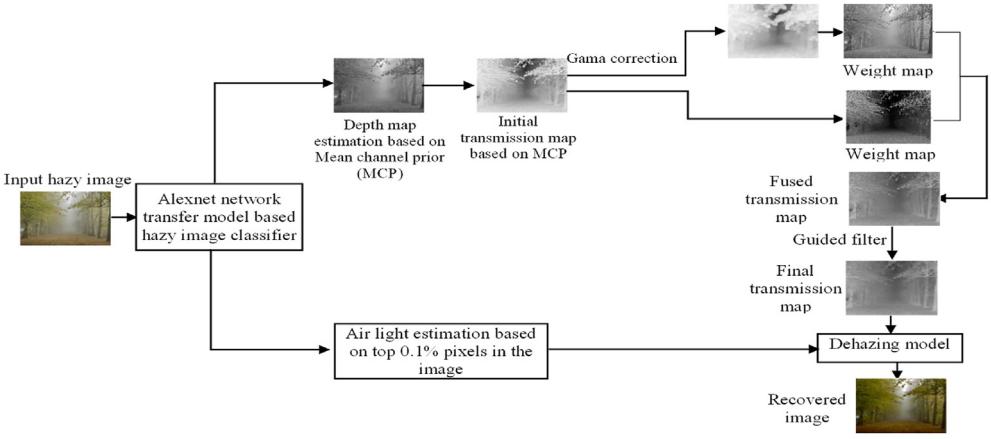

Fig. 1. The proposed block diagram.

subjected to a guided filter. Finally, using the obtained transmission map and an optical scattering model, the dehazed images are recovered.

3.1. Alexnet network transfer model-based hazy image classifier

3.1.1. Alexnet - Convolution neural network

Krizhevzky and others suggested the concept of Alexnet. AlexNet's image recognition precision is more than twice that of ImageNet, and it possesses unique benefits. It is the most traditional model in the domain of digital imaging [28,29]. Alexnet's network architecture consists of eight layers, five of which are convolution layers and three of which are fully connected. Up to 1000 different types of image categorization may be done by training the network using massive amounts of data. Table 1 shows the Alexnet architecture.

The dimensions of the input image for the network are 227 × 227 × 3. The value 227 corresponds to both the height and width of the image, while the value 3 signifies that the image is in RGB format, consisting of three color channels. To ensure consistency throughout training, it is necessary to normalize the size of the training pictures to 227 × 227 pixels. In the standard Alexnet network, the first and second layers are followed by the max pooling layer, normalization layer, and ReLu activation function. The third layer utilizes the convolution layer and ReLu activation function, while the fifth layer is identical to the first layer but lacks normalization by the norm. The fully connected layers are layers six to eight, while the final layer employs a softmax classifier to classify the images by 1000.

3.1.2. Transfer model-based haze image classification

It is generally known that standard ANN models often need a lot of data to make more accurate models. Similarly, using Alexnet for image classification requires many training data sets to reach a better precision [30]. However, getting training data for a public modeling assignment is frequently challenging. Overusing training sets can enhance precision rates, increase the complexity of network

Table 1. Alexnet network architecture using CNN.

Layer		Feature map	Size	Kernel size	Stride	Activation
Input	image	1	227 × 227 × 3	–	–	–
1	Convolution	96	55 × 55 × 96	11 × 11	4	relu
	Max pooling	96	27 × 27 × 96	3 × 3	2	relu
2	Convolution	256	227 × 227 × 256	5 × 5	1	relu
	Max pooling	256	13 × 13 × 256	3 × 3	2	relu
3	Convolution	384	13 × 13 × 384	3 × 3	1	relu
4	Convolution	384	13 × 13 × 384	3 × 3	1	relu
5	Convolution	256	13 × 13 × 256	3 × 3	1	relu
	Max pooling	256	6 × 6 × 256	3 × 3	2	relu
6	FC	–	9216	–	–	relu
7	FC	–	4096	–	–	relu
8	FC	–	4096	–	–	relu
Output	FC	–	1000	–	–	softmax

training, and introduce the problem of over-fitting. This paper suggests a hazy image classification technique based on Alexnet network transfer to improve precision and reduce training difficulty.

As depicted in Fig. 2, the source task (ImageNet classification task) is used to train the AlexNet network and evaluate its training precision. Then, move the last three elements to the target task (hazy image recognition task) to achieve network element transfer. When the elements of the original network are transferred to the target task, the new network needs to be trained. The classification precision can be improved by repeatedly modifying the elements because of the differences between the transferred network's dataset (Datasets 1 and 2) and the original network.

3.2. Mean channel prior

This paper introduced an essential prior for transmission map estimation using MCP. According to a comprehensive study utilizing some hazy datasets, such as the Reside dataset, released in 2017, available at https://sites.google.com/view/reside-dehaze-datasets/reside-standard; FRIDA dataset, released in 2010, available at http://perso.lcpc.fr/tarel.jean-philippe/bdd/frida; and D-HAZY dataset, released in 2016, available at https://paperswithcode.com/dataset/d-hazy. The three channels' mean value increases continuously with the haze level. Based on a statistical analysis of the histograms depicting the mean value of the hazy image and ground truth, it was determined that there is a positive correlation between haze concentration (precisely, depth) and the mean channel value. Also, the distribution of mean pixel values throughout the whole scale. It can be seen clearly that 75% of the pixel values are below 0.6. However, when the concentration of haze grows, the mean pixel values tend to concentrate at higher values. The mean channel of the hazy images may be computed using the following formula:

$$M_{ch} = \left(\underset{c=R,G,B}{mean} I^{C}(i,j) \right) \tag{4}$$

Where I is the hazy image, i,j is the pixels index, and M_{ch} denotes the mean channel, which can roughly be described as a depth map representing the hazing intensity. The transmission map may be computed using Equation (5) based on the atmospheric scattering model.

$$t(i,j) = e^{-\beta(M_{ch})} \tag{5}$$

Where β is the attenuation parameter, which is sensitivity to wavelengths and, therefore, different for the three color channels, and M_{ch} is the depth map derived from the MCP.

3.3. Gamma correction for transmission map

The gamma correction equation to calculate the transmission map is defined as follows.

$$T_2(i) = T_1(i)^{\frac{1}{\lambda}} \tag{6}$$

$T_1(x)$ stands for the original transmission map derived from Equation (5). Fig. 3 shows two lines with $\lambda = 1$ and 4. For $\lambda = 4$, the image's dynamic range increases in the low gray value region, increasing the image's contrast. Conversely, the dynamic range decreases in the large gray value area, resulting in lower contrast in the image.

3.4. Adaptive image fusion for transmission map estimation

This paper employed a weighted average image fusion technique of different transmission estimation strategies for normal and bright regions to enhance the precision of transmission map calculation. The transmission map obtained by MCP is

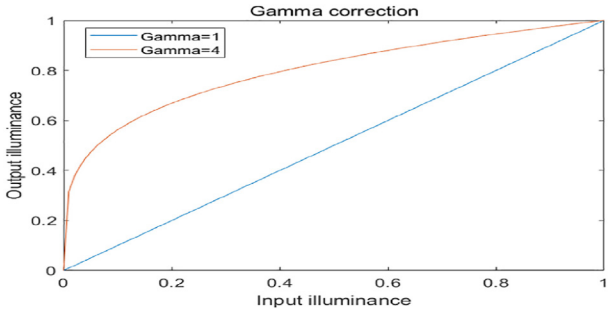

Fig. 3. Gamma correction curve.

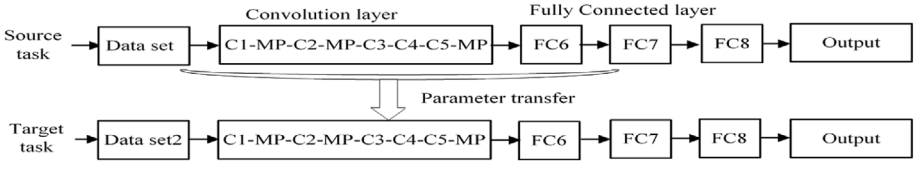

Fig. 2. Transfer learning-based Network model.

generally excellent in typical areas. Therefore, a greater weight is assigned to the first transmission map produced by MCP and a lower weight to its corrected map. However, in bright regions, the transmission map produced by MCP is always inflated. Therefore, the original transmission map is assigned a lower and higher weight to its corrected map. Consequently, the fusion formula can be defined as follows.

$$T_F(i) = T_1(i)W_F(i) + T_2(i)(1 - W_F(i)) \quad (7)$$

Where T_1(i) is the transmission map produced by MCP, T_2(i) is the transmission handled by Gamma correction. W_F(i) represents the fusion weighting and the computation process, illustrated in Fig. 4.

The transmission map estimated by MCP (original) and its corrected map is first filtered using a guided filter.

$$G_1(i) = GuidF_{\tau,\epsilon}(T_1(i)) \quad (8)$$

$$G_2(i) = GuidF_{\tau,\epsilon}(T_2(i)) \quad (9)$$

The weighting is then created by.

$$W_F(i) = \frac{T_1(i)T_2(i)}{(G_1(i) + a)(G_2(i) + a)} \quad (10)$$

Where a is a variable value defined by.

$$a = \frac{Max\left(I^{dark}(i)\right)}{K} \quad (11)$$

Where k is a fixed value, the proposed approach adaptively restores various hazy photos by calculating adaptive weighting maps. Next, a guided filter is employed on the fused transmission map to improve its visible effect performance, thereby resolving the halo issue and blocking artifacts of the dazed image.

$$T_F(i) = GuidF_{\tau,\epsilon}(I^{gray}(i), T_F(i)) \quad (12)$$

I^{gray}(i) is the original image's grey map (guided map).

3.5. Atmospheric light calculation

Estimating airlight (A) is another crucial aspect of haze model processing (3). According to the haze model, there is a remarkable relationship between haze concentration and brightness. As the haze concentration increases, the image's brightness increases, too. The air light, denoted by (A) in Ref. [5], corresponds to the maximum value of the input image. Nevertheless, it is worth noting that there are instances where images may contain white items that appear brighter than the real object. It could lead to inaccurate estimations. This study estimated air light by calculating the average value of the top 0.1% pixels inside the dark channel, as referenced in Ref. [14]. The calculation of the dark track may be determined as follows.

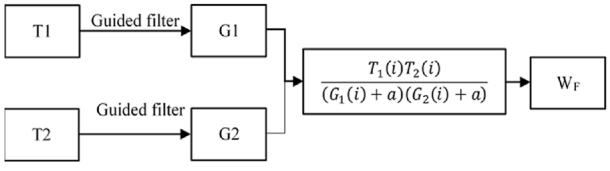

Fig. 4. A flowchart for calculating the weighting map.

$$J_{dark}(i) = \left(\min_{c=R,G,B} J^C(i)\right) \quad (13)$$

J_{dark} (i) is the lowest channel in the input J(i). Using (9) as a basis, air light can be computed as follows:

$$A = \frac{\sum_{i=0}^{n} J_{dark}(i)}{n} \quad (14)$$

Where n is the number of pixels in Jdark (i) that correspond to the top 0.1% in brightness, arranged in ascending order.

3.6. Scene radiance recovery

Upon performing the necessary calculations for the airlight and transmission map, the scene irradiance has been successfully recreated from (1). The final scene irradiance recovery can be achieved by implementing Equation (11); by rearranging Equation (1), the ground truth J(i,j) can be expressed as.

$$J(i) = \frac{I(i) - A}{T_F(i)} + A \quad (15)$$

4. Experimental results and discussion

In this section, the classification of hazy images is discussed first. Then, the free parameters are set up. Finally, the performance of the suggested method is compared with the eight latest or classical approaches on both authentic and synthetic images. The eight methods are He et al. [2], Berman et al. [31], Dhara et al. [32], Zheng et al. [33], Zhang and Patel [34], Ju et al. [35], Zhu et al. [19], Cai et al. [26].

4.1. Hazy image classification

In the experiment, 700 images were used as experimental data, selected from different repositories, including RESIDE, FRIDA, D-HAZY, and

Google. These images consist of 350 hazy images and 350 free images. To prevent the overlapping and merging of the training set and test set, 700 images were randomly shuffled. Three hundred fifty images were randomly chosen from this pool to form the training set, while the remaining 100 images were designated as the test set. The number of categories in the Alexnet network has been reduced from 1000 to 2. The network is configured to undergo 7 epochs, each with 14 training iterations. This process is repeated 97 times in all. The first learning rate for the network is established at 0.002. Each iteration's learning rate is automatically halved. Fig. 5 and Table 2 show the experimental results.

The results indicate that the training precision can attain a value of 1 while the accuracy in the test set can achieve 0.98. Based on the results shown in Fig. 5 and Table 2, it is clear that the precision curves for the training set and the test set show a high degree of similarity. This indicates the absence of over-fitting, as indicated by precision values close to 1 and 0.97, respectively.

4.2. Parameter settings

The parameters τ ε in equations (8) and (9) are determined by empirical methods, with values of 15 and 0.001 selected. Gamma in (6) and k in (11) have significant implications in the context of the suggested objective metrics. They are called PSNR and SSIM, respectively. Consequently, a series of tests were conducted to examine the optimal values for the parameter.

Firstly, k is changed from 1 to 8, and Gamma is set to 4. Fig. 6 illustrates the results of PSNR and SSIM on a selection of images taken from the open-source dataset RESIDE. Fig. 6(a) and (c) illustrate the PSNR and SSIM objective metrics line charts when k is about 3. Both objective metrics provide the highest

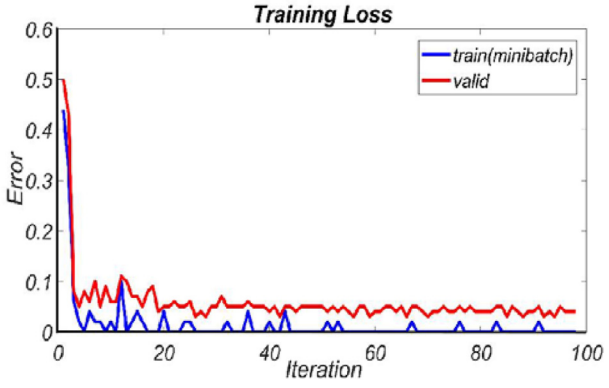

Fig. 5. Training and validation precision.

Table 2. Training and validation precision.

Epoch	Learning rate	Precision	
		Training precision	Test precision
1	0.002	0.98	0.92
2	0.002	1	0.93
3	0.002	1	0.95
4	0.001	1	0.96
5	0.001	1	0.97
6	0.001	1	0.97
7	0.005	1	0.97

results. Then, k is set to three, and Gamma is adjusted from one to eight. Fig. 6(b) and (d) illustrate the PSNR and SSIM objective metrics with Gamma values ranging from one to eight. When the value of Gamma attains 4, it is clear that the PSNR and SSIM performances stay stable. As a result, in the proposed technique, k and Gamma were set to 3 and 4, respectively.

4.3. A comparative analysis of subjective perceptions between real and synthetic images

Five real-world hazy images labeled RI_1, RI_2, RI_3, RI_4, RI_5 and five synthetic images labeled SI_1, SI_2, SI_3, SI_4, and SI_5 were chosen from RESIDE dataset, FRIDA dataset, and D-HAZY dataset for comparison analysis, and the results are explained in Fig. 7 and Fig. 8, respectively. In Figs. 7 and 8, He et al. [2] demonstrate effective dehazing, but it has been observed that the He et al. approach [2] is not applicable in the white and sky areas, which results in color distortion and excessive enhancement in these regions. This issue is evident in images RI_3, RI_5, SI_1, SI_3, and SI_4. Similarly, the dehazed outcomes obtained by the approach proposed by Berman et al. [31] exhibited excessive enhancement. It can be attributed to the inaccurate calculation of the transmission map for specific images, as exemplified by RI_3, RI_4, and RI_5. Dhara et al. [32] proposed a color correction technique inspired by the method developed by He et al. [2]. This approach demonstrates significant efficacy in addressing the issue of color distortion. Hence, the visual outcome of dehazed images achieved by the method proposed by Dhara et al. [32] is deemed suitable. The methodologies proposed by Zheng et al. [33] and Zhang et al. [34] both center around image enhancement. Despite exhibiting dehazing solid capabilities, the dehazed results are marred by artifact colors. This issue arises from the heavy reliance on the improved images, as evidenced by color artifacts in images RI_1, RI_3, RI_4, and SI_1. The dehazed outcomes obtained from the method proposed by Ju et al. [35] exhibit noticeable over-lightning. The enhancement

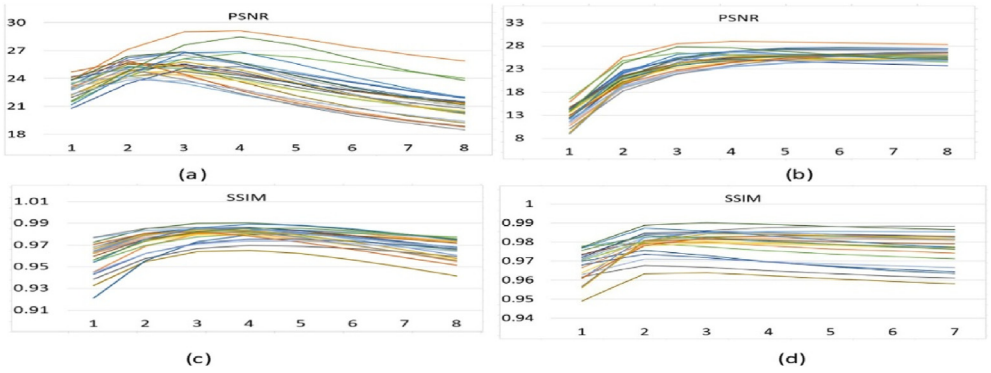

Fig. 6. The PSNR and SSIM of the dehazed images using various settings (k and Gamma) (a) PSNR with different k, (b) PSNR with different Gamma, (c) SSIM with different k, and (d) SSIM with different Gamma.

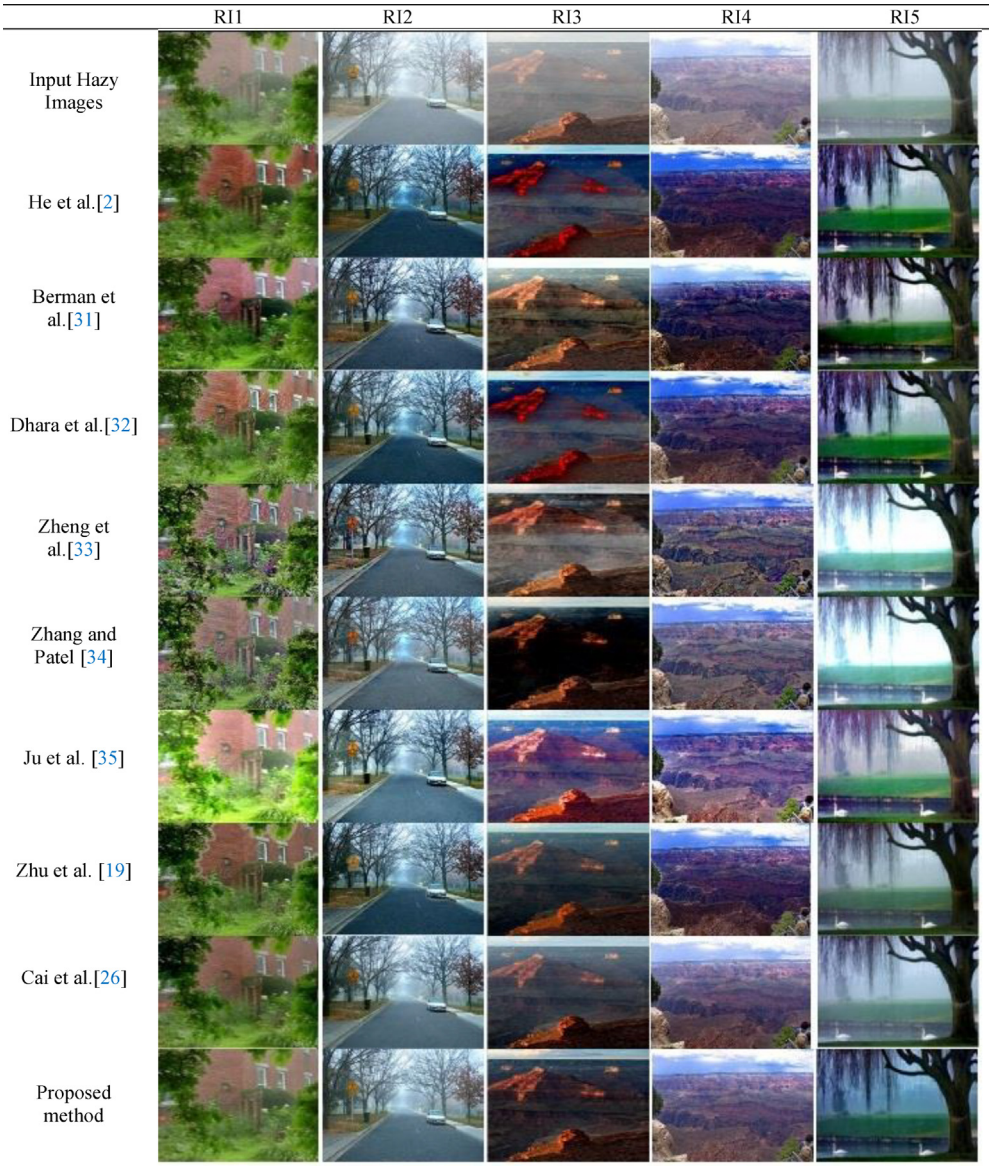

Fig. 7. Result of different dehazing methods and proposed method on real-world images.

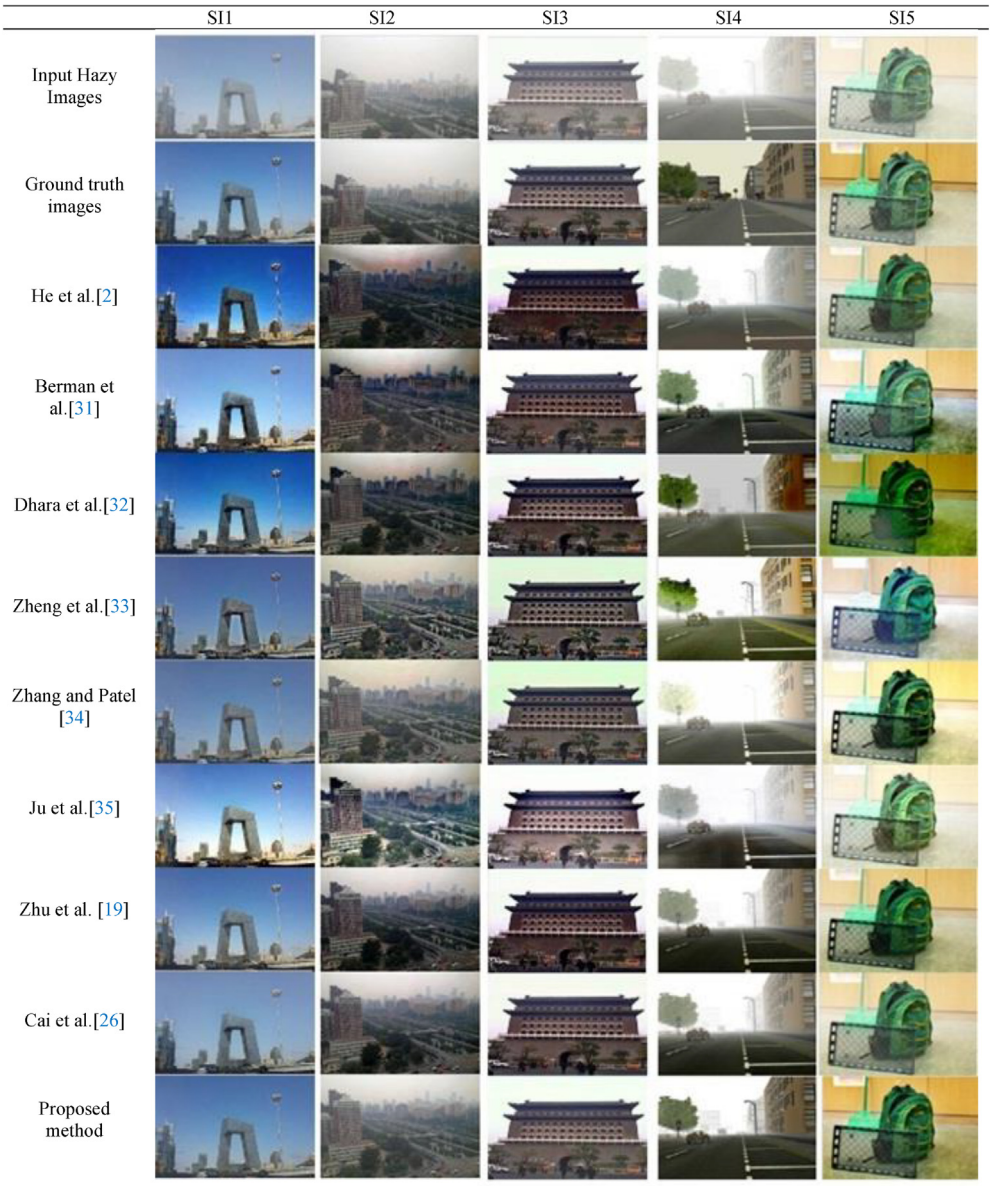

Fig. 8. Result of different dehazing methods and proposed method on synthetic images.

of overall brightness in the atmospheric scattering model (ASM) results can be attributed to introduce the light absorption coefficient. Collectively, the approach proposed by Zhu et al. [19], the method proposed by Cai et al. [26], and the method proposed in this study demonstrate effective haze removal capabilities in source images. Additionally, the colors of recovered images are realistic and natural.

4.4. A comparative analysis of quantitative perceptions

Given the inherent subjectivity of individual viewers' judgments, the introduction of objective indicators serves the purpose of quantitatively evaluating the performances of various methodologies. The indicators encompassed in this study are the natural image quality evaluator (NIQE) [36], the peak signal-to-noise ratio (PSNR) [37], and the measure of structural similarity (SSIM) [38]. One of the non-reference indicators is NIQE. The degree of realism and naturalness of restored images is inversely proportional to the magnitude of the NIQE metric. Table 3 presents the NIQE index values obtained from evaluating several dehazing techniques on real-world images. The instances highlighted in bold indicate the highest quality according to the Natural Image Quality Evaluator (NIQE). At the same time, those underlined

Table 3. Comparison of the proposed method with different methods in terms of NIQE on real-world images.

Image	He et al. [2]	Berman et al. [31]	Dhara et al. [32]	Zheng et al. [33]	Zhang et al. [34]	Ju et al. [35]	Zhu et al. [19]	Cai et al. [26]	proposed method
NI_1	2.548	2.697	2.624	2.561	2.659	2.643	2.713	2.685	2.607
NI_2	2.478	2.417	2.408	2.594	2.521	2.43	2.43	2.543	2.409
NI_3	2.287	2.143	2.381	2.379	2.609	2.297	2.411	2.482	2.5
NI_4	1.955	1.829	1.824	2.075	1.957	1.767	1.922	1.903	1.925
NI_5	2.785	3.028	2.661	3.479	3.241	2.63	2.519	2.459	2.49
Average	2.411	2.423	2.380	2.618	2.597	2.353	2.399	2.414	2.386

Table 4. Comparison of the proposed method with different methods in terms of PSNR on the synthetic images.

Image	He et al. [2]	Berman et al. [31]	Dhara et al. [32]	Zheng et al. [33]	Zhang and Patel [34]	Ju et al. [35]	Zhu et al. [19]	Cai et al. [26]	Proposed method
SI_1	17.384	19.501	20.585	20.338	22.532	18.508	19.365	25.196	29.596
SI_2	16.951	18.587	19.09	17.877	19.373	21.559	22.152	22.839	28.004
SI_3	11.567	13.058	13.002	18.702	22.129	15.962	16.625	19.734	28.17
SI_4	15.976	19.634	25.755	19.981	25.744	17.397	21.739	24.25	26.262
SI_5	15.94	18.321	18.041	20.366	24.478	17.144	32.64	22.877	26.628
Average	15.564	17.820	19.295	19.453	22.851	18.114	22.504	22.979	27.732

represent the second highest quality as determined by the same metric. According to the data presented in Table 3, our method demonstrates an average NIQE ranked second, with only Dhara et al.'s method [32] achieving a lower score. The Normalized Image Quality Evaluations (NIQEs) of the methods proposed by Zheng et al. [33] and Zhu et al. [19] exhibit high values due to the presence of noticeable color distortion in their dehazed output. The dehazed outcomes obtained from the methodologies proposed by He et al. [2], Berman et al. [31], and Ju et al. [35] tend to excessive enhancement.

Consequently, the average NIQE of the group above is comparatively elevated. In general, the method proposed by Zhu et al. [19], the method proposed by Dhara et al. [32], and the method proposed in this study demonstrate the ability to achieve relatively low Natural Image Quality Evaluator (NIQE) scores. It can be attributed to the fact that the dehazed images produced by these methods exhibit a higher degree of realism than other approaches.

PSNR is a metric that quantifies the relationship between an image's highest achievable power and the noise power that compromises the precision of the signal representation [38]. The formula can be expressed as.

$$PSNR = 10\log_{10}\left[\frac{MAX^2_{I_{HF}(i)}}{MSE}\right] \tag{16}$$

Where I_{HF} (i) is the clear image, and MAX^2_{IHF}(i) denotes the square of the highest pixel value in I_{HF} (i). MSE is the mean square error as:

Table 5. Comparison of the proposed method with different methods in terms of SSIM on the synthetic images.

Image	He et al. [2]	Berman et al. [31]	Dhara et al. [32]	Zheng et al. [33]	Zhang and Patel [34]	Ju et al. [35]	Zhu et al. [19]	Cai et al. [26]	Proposed method
SI1	0.882	0.945	0.923	0.683	0.938	0.983	0.971	0.964	0.969
SI2	0.907	0.940	0.944	0.905	0.889	0.974	0.950	0.942	0.988
SI3	0.715	0.766	0.895	0.933	0.808	0.936	0.841	0.943	0.990
SI4	0.845	0.914	0.926	0.909	0.943	0.962	0.938	0.929	0.981
SI5	0.857	0.928	0.962	0.784	0.934	0.981	0.988	0.959	0.984
Average	0.841	0.899	0.930	0.843	0.902	0.967	0.938	0.947	0.982

Table 6. Average values of PSNR and SSIM for RESIDE dataset.

Metrics	He et al. [2]	Berman et al. [31]	Dhara et al. [32]	Zheng et al. [33]	Zhang and Patel [34]	Ju et al. [35]	Zhu et al. [19]	Cai et al. [26]	Proposed method
PSNR	14.678	18.059	17.166	18.368	19.512	15.524	19.993	22.627	**22.668**
SSMI	0.819	0.873	0.886	0.851	0.888	0.820	0.870	0.918	**0.930**

The values in bold represent the best PSNR and SSIM. Our method achieves better results compared to other methods.

$$MSE = \frac{1}{w \times h}\sum_{i=1}^{w}\sum_{j=1}^{h}(J(i) - \mathrm{I}_{HF}(i))^2 \quad (17)$$

Where h and w are height and width, respectively, and J (i) is the dehazing result. The SSIM index quantifies the degree of similarity between dehazing images and clear images. It assesses the outcomes in three areas: lighting l(i), contrast c(i), and structure s(i).

$$SSIM = f(\mathrm{l}(i), \mathrm{c}(i), \mathrm{s}(i)) \quad (18)$$

The utilization of PSNR and SSIM as reference metrics necessitates the comparison of dehazing outcomes with haze-free images. Hence, the employment of PSNR and SSIM is limited to the exclusive assessment of synthetic images. Greater values of PSNR and SSIM indicate superior performance in the dehazing outcomes. Tables 4 and 5 present the PSNR and SSIM metrics for synthetic images. Tables 6–8 show the average performance for the RESIDE, FRIDA, and D-HAZY datasets.

4.5. A comparative analysis of time complexity

Table 9 depicts the proposed approach's time consumption and the comparative approaches across different image sizes (excluding the computing time required for the classifier). The studies by Zhu et al. [19] and Zheng et al. [33] use a multi-exposure fusion method to accomplish image dehazing. The authors of Zheng et al. [33] proposed an adaptive structural decomposition combined for every image patch in their fusion model. However, this approach exhibits a relatively high computation complexity, increasing processing time. In the study conducted by He et al. [2], soft matting was employed to enhance the precision and quality of the transmission map.

All the same, using soft matting significantly augmented the total duration of the execution process. Dhara et al. [32] proposed using color correction as an alternative to soft matting to enhance the precision of transmission map estimates. This approach has the potential to cut processing time to a certain extent. The study conducted by Cai et al. [26] showed that using deep networks for estimating transmission maps increased the overall execution time, primarily due to the extensive parameter computations involved. The k-means technique was utilized by Berman et al. [31] to cluster pixels into a haze line and subsequently estimate the transmission map using the haze line. Meanwhile, a sparsely populated linear system, known for its time-consuming nature, was employed to enhance the transmission map, resulting in a corresponding increase in the overall execution duration. According to the data presented in Table 9, it is evident that the suggested method exhibits the shortest duration of consumption for source images of varying sizes.

Table 7. Average values of PSNR and SSIM for the FRIDA dataset.

Metrics	He et al. [2]	Berman et al. [31]	Dhara et al. [32]	Zheng et al. [33]	Zhang and Patel [34]	Ju et al. [35]	Zhu et al. [19]	Cai et al. [26]	Proposed method
PSNR	15.285	17.942	16.265	18.223	21.512	18.511	19.325	20.329	**21.432**
SSMI	0.711	0.767	0.854	0.822	0.847	0.824	0.877	0.932	**0.951**

The values in bold represent the best PSNR and SSIM. Our method achieves better results compared to other methods.

Table 8. Average values of PSNR and SSIM for the D-HAZY dataset.

Metrics	He et al. [2]	Berman et al. [31]	Dhara et al. [32]	Zheng et al. [33]	Zhang and Patel [34]	Ju et al. [35]	Zhu et al. [19]	Cai et al. [26]	Proposed method
PSNR	16.586	16.610	17.166	18.368	19.112	15.524	14.45	14.72	**19.254**
SSMI	0.865	0.750	0.868	0.851	0.866	0.825	0.785	0.791	**0.873**

The values in bold represent the best PSNR and SSIM. Our method achieves better results compared to other methods.

Table 9. Comparison of the proposed method with different methods in terms of time complexity.

Image	He et al. [2]	Berman et al. [31]	Dhara et al. [32]	Zheng et al. [33]	Zhang and Patel [34]	Ju et al. [35]	Zhu et al. [19]	Cai et al. [26]	Proposed method
3346 × 2032	19.501	11.456	29.788	31.936	20.896	2 19.493	6.317	23.709	4.358
1200 × 992	3.389	6.055	8.337	5.599	4.375	37.928	1.025	3.210	0.705
1024 × 668	1.972	3.488	5.533	3.287	2.599	21.699	0.575	1.750	0.373
768 × 497	1.198	1.781	4.992	1.906	1.329	12.395	0.329	1.338	0.208
400 × 450	0.632	1.075	4.706	1.023	0.807	6.627	0.208	0.804	0.113
398 × 265	0.374	0.745	4.338	0.677	0.376	3.176	0.170	0.441	0.045
Average	4.511	4.771	9.616	7.405	5.064	50.220	1.437	5.209	0.967

5. Conclusion

This paper presents an Alexnet hazy image classification network for automated hazy image identification, and it is executed and obtained a verification precision of 93.4% over 50 epochs. Also, a practical approach for image dehazing was introduced based on estimating the transmission map and fusion strategy. This technique is based on the MCP, which has a solid theoretical foundation and good dehazing results. This paper intends to address the issue of a color shift in the sky and white regions in MCP while preserving dehazing performance. Therefore, it preprocesses the transmission map acquired from the MCP using gamma correction. Then, an adaptive fusion strategy can be proposed to combine the corrected image with the MCP-obtained initial transmission image. Adaptively fusing an approach that preserves the details in recovered images and aims for various levels of image haziness is effective and adaptive. Finally, a guided filter is employed for the fused transmission map to eliminate the block and halo effects of the sky region. It uses PSNR, SSIM, and NIQE to assess the effectiveness of image recovery. This paper compares the proposed method to the eight latest and classic methods on real-world and synthetic haze images. Additionally, time complexity is compared. Based on the obtained results, the proposed method can effectively address the issue of color shift of the recovered image and its computation speed.

Conflict of interest

The authors declare that they have no conflict of interest, and they all agree to publish this paper under academic ethics.

Author contributions

All the authors contributed equally to the manuscript.

Funding

The Babylon University and Wasit University are supported this work.

Acknowledgments

We express our deep appreciation to the faculty of Information Technology College and Engineering College, Babylon University. In addition, we appreciate the cooperation from the Electrical Engineering Department in Wasit for their patient guidance, enthusiastic encouragement, and valuable critiques of this research work.

References

[1] S.G. Narasimhan, S.K. Nayar, Vision and the atmosphere, Int J Comput Vis 48 (3) (2002) 233–254, https://doi.org/10.1023/A:1016328200723.
[2] K. He, J. Sun, X. Tang, Single image haze removal using dark channel prior, IEEE Trans Pattern Anal Mach Intell 33 (12) (2010) 2341–2353, https://doi.org/10.1109/TPAMI.2010.168.
[3] W. Wang, X. Yuan, X. Wu, Y. Liu, Fast image dehazing method based on linear transformation, IEEE Trans Multimed 19 (6) (2017) 1142–1155, https://doi.org/10.1109/TMM.2017.2652069.
[4] A. Khmag, S.A.R. Al-Haddad, R.A.R. amli, B. Kalantar, Single image dehazing using second-generation wavelet transforms and the mean vector L2-norm, Vis Comput 34 (5) (2018) 675–688, https://doi.org/10.1007/s00371-017-1406-5.
[5] H. Kumar, S. Gupta, K.S. Venkatesh, Realtime dehazing using colour uniformity principle, IET Image Process 13 (11) (2019) 1931–1939, https://doi.org/10.1049/iet-ipr.2018.5240.
[6] Y. Gao, H. Chen, H. Li, W. Zhang, Single image dehazing using local linear fusion, IET Image Process 12 (5) (2018) 637–643, https://doi.org/10.1049/iet-ipr.2017.0570.
[7] A. Khmag, Image dehazing and defogging based on second-generation wavelets and estimation of transmission map, Multimed Tool Appl 82 (29) (2023) 1–17, https://doi.org/10.1007/s11042-023-17819-z.
[8] S.G. Narasimhan, S.K. Nayar, Contrast restoration of weather degraded images, IEEE Trans Pattern Anal Mach Intell 25 (6) (2003) 713–724, https://doi.org/10.1109/TPAMI.2003.1201821.
[9] A.M. Reza, Realization of the contrast limited adaptive histogram equalization (CLAHE) for real-time image enhancement, J. VLSI Signal Process Syst Signal, Image Video Technol 38 (1) (2004) 35–44, https://doi.org/10.1023/B:VLSI.0000028532.53893.82.
[10] S. Oishi, N. Fukushima, Retinex-based relighting for night photography, Appl Sci 13 (3) (2023) 1–19, https://doi.org/10.3390/app13031719.
[11] A. Kumari, S.K. Sahoo, Real time visibility enhancement for single image haze removal, Procedia Comput Sci 54 (2015) 501–507, https://doi.org/10.1016/j.procs.2015.06.057.
[12] R. Fattal, Single image dehazing, ACM Trans Graph 27 (3) (2008) 1–9, https://doi.org/10.1145/1360612.1360671.
[13] K. He, J. Sun, X. Tang, Guided image filtering, IEEE Trans Pattern Anal Mach Intell 35 (6) (2012) 1397–1409, https://doi.org/10.1109/TPAMI.2012.213.
[14] D. Jang, R. Park, Colour image dehazing using near-infrared fusion, IET Image Process 11 (8) (2017) 587–594, https://doi.org/10.1049/iet-ipr.2017.0192.
[15] D. Nair, P. Sankaran, Color image dehazing using surround filter and dark channel prior, J Vis Commun Image Represent 50 (1) (2018) 9–15, https://doi.org/10.1016/j.jvcir.2017.11.005.
[16] Z. Gu, M. Ju, D. Zhang, A single image dehazing method using average saturation prior, Math Probl Eng 2017 (1) (2017) 1–17, https://doi.org/10.1155/2017/6851301.
[17] R. He, Z. Wang, Y. Fan, D.D. Feng, Combined constraint for single image dehazing, Electron Lett 51 (22) (2015) 1776–1778, https://doi.org/10.1049/el.2015.0707.
[18] G. Meng, Y. Wang, J. Duan, S. Xiang, C. Pan, Efficient image dehazing with boundary constraint and contextual regularization, Proc IEEE Int Conf Comput Vis (2013) 617–624, https://doi.org/10.1109/ICCV.2013.82.
[19] Q. Zhu, J. Mai, L. Shao, A fast single image haze removal algorithm using color attenuation prior, IEEE Trans Image Process 24 (11) (2015) 3522–3533, https://doi.org/10.1109/TIP.2015.2446191.
[20] Q. Liu, X. Gao, L. He, W. Lu, Single image dehazing with depth-aware non-local total variation regularization, IEEE Trans Image Process 27 (10) (2018) 5178–5191, https://doi.org/10.1109/TIP.2018.2849928.
[21] K.B. Gibson, T.Q. Nguyen, Fast single image fog removal using the adaptive Wiener filter, in: 2013 IEEE International

Conference on Image Processing, IEEE. 2013, pp. 714–718, https://doi.org/10.1109/ICIP.2013.6738147.
[22] L. Zhang, S. Wang, X. Wang, Saliency-based dark channel prior model for single image haze removal, IET Image Process 12 (6) (2018) 1049–1055, https://doi.org/10.1049/iet-ipr.2017.0959.
[23] F. Yuan, H. Huang, Image haze removal via reference retrieval and scene prior, IEEE Trans Image Process 27 (9) (2018) 4395–4409, https://doi.org/10.1109/TIP.2018.2837900.
[24] G. Sahu, A. Seal, Image dehazing based on luminance stretching, in: 2019 International Conference on Information Technology (ICIT), IEEE. 2019, pp. 388–393, https://doi.org/10.1109/ICIT48102.2019.00075.
[25] A. Khmag, Smoke removal technique of industrial scene images based on second-generation wavelets and dark channel prior model, Soft Comput 27 (23) (2023) 17505–17514, https://doi.org/10.1007/s00500-023-09204-7.
[26] B. Cai, X. Xu, K. Jia, C. Qing, D. Tao, Dehazenet: an end-to-end system for single image haze removal, IEEE Trans Image Process 25 (11) (2016) 5187–5198, https://doi.org/10.1109/TIP.2016.2598681.
[27] S. Santra, R. Mondal, B. Chanda, Learning a patch quality comparator for single image dehazing, IEEE Trans Image Process 27 (9) (2018) 4598–4607, https://doi.org/10.1109/TIP.2018.2841198.
[28] A. Krizhevsky, I. Sutskever, G.E. Hinton, ImageNet classification with deep convolutional neural networks, Commun ACM 60 (6) (2017) 84–90, https://doi.org/10.1145/3065386.
[29] S. Dutta, B.C. Manideep, S.M. Basha, R.D. Caytiles, N.C.S.N. Iyengar, F. LI, Classification of diabetic retinopathy images by using deep learning models, Int J Grid Distrib Comput 11 (1) (2018) 89–106, https://doi.org/10.14257/ijgdc.2018.11.1.09.
[30] T.J. Saleem, S.R. Zahra, F. Wu, A. Alwakeel, M. Alwakeel, F. Jeribi, M. Hijji, Deep learning-based diagnosis of Alzheimer's disease, J Personalized Med 12 (5) (2022) 815, https://doi.org/10.3390/jpm12050815.
[31] D. Berman, T. Treibitz, S. Avidan, Single image dehazing using haze-lines, IEEE Trans Pattern Anal Mach Intell 42 (3) (2018) 720–734, https://doi.org/10.1109/TPAMI.2018.2882478.
[32] S.K. Dhara, M. Roy, D. Sen, P.K. Biswas, Color cast dependent image dehazing via adaptive airlight refinement and non-linear color balancing, IEEE Trans Circ Syst Video Technol 31 (5) (2020) 2076–2081, https://doi.org/10.1109/TCSVT.2020.3007850.
[33] M. Zheng, G. Qi, Z. Zhu, Y. Li, H. Wei, Y. Liu, Image dehazing by an artificial image fusion method based on adaptive structure decomposition, IEEE Sensor J 20 (14) (2020) 8062–8072, https://doi.org/10.1109/JSEN.2020.2981719.
[34] H. Zhang, V.M. Patel, Densely connected pyramid dehazing network, in: Proceedings of the IEEE Conference on Computer Vision and Pattern Recognition (CVPR), 2018, pp. 3194–3203, https://doi.org/10.48550/arXiv.1803.08396.
[35] M. Ju, C. Ding, W. Ren, Y. Yang, D. Zhang, Y.J. Guo, IDE: image dehazing and exposure using an enhanced atmospheric scattering model, IEEE Trans Image Process 30 (2021) 2180–2192, https://doi.org/10.1109/TIP.2021.3050643.
[36] A. Mittal, R. Soundararajan, A.C. Bovik, Making a "completely blind" image quality analyzer, IEEE Signal Process Lett 20 (3) (2012) 209–212, https://doi.org/10.1109/LSP.2012.2227726.
[37] Z. Wang, A.C. Bovik, H.R. Sheikh, E.P. Simoncelli, Image quality assessment: from error visibility to structural similarity, IEEE Trans Image Process 13 (2004) 600–612, https://doi.org/10.1109/TIP.2003.819861.
[38] A. Hore, D. Ziou, Image quality metrics: PSNR vs. SSIM, in: Proceedings of the IEEE International Conference on Computer Vision (ICCV), IEEE. 2010, pp. 2366–2369, https://doi.org/10.1109/ICPR.2010.579.